



Gapped phase in AA-stacked bilayer graphene

L. Brey¹ and H. A. Fertig²

¹*Instituto de Ciencia de Materiales de Madrid, (CSIC), Cantoblanco, E-28049 Madrid, Spain*

²*Department of Physics, Indiana University, Bloomington, Indiana 47405, USA*

(Received 21 December 2012; published 12 March 2013)

AA-stacked bilayer graphene supports Fermi circles in its bonding and antibonding bands, which coincide exactly, leading to symmetry breaking in the presence of electron-electron interactions. We analyze a continuum model of this system in the Hartree-Fock approximation, using a self-consistently screened interaction that accounts for the gap in the spectrum in the broken symmetry state. The order parameter in the ground state is shown to be of the Ising type, involving transfer of charge between the layers in opposite directions for different sublattices. We analyze the Ising phase transition for the system and argue that it continuously evolves into a Kosterlitz-Thouless transition in the limit of vanishing interlayer separation d . The transition temperature is shown to depend only on the effective spin stiffness of the system even for $d > 0$, and an estimate of its value suggests that the transition temperature is of the order of a few degrees Kelvin.

DOI: [10.1103/PhysRevB.87.115411](https://doi.org/10.1103/PhysRevB.87.115411)

PACS number(s): 61.46.—w, 73.22.Pr, 73.63.—b

I. INTRODUCTION

Graphene is a two-dimensional triangular lattice of carbon atoms with two sublattice atoms, A and B, in each unit cell, forming a honeycomb structure. Its electronic low-energy properties are governed by a massless Dirac Hamiltonian, and near the neutrality point the quasiparticle energies disperse linearly with a speed v_F .¹ Coulomb interactions in this system can be characterized by an effective fine-structure constant $\beta = e^2/\epsilon\hbar v_F$, where ϵ is a dielectric constant due to the substrate upon which graphene is deposited. For moderate values of β , electron-electron interactions renormalize the speed of the carriers near the Dirac points, but do not alter the semimetallic character of the spectrum.^{2,3} For larger values of β ($\beta \sim 1$), theoretical studies indicate that the Coulomb interaction becomes important,^{3–6} and there is the possibility of a gap opening in the spectrum due to dynamical symmetry breaking. At the present, there is no evidence for such a gap under experimentally realizable circumstances.

The situation becomes dramatically different when one considers two-layer graphene systems.⁷ Under most circumstances, graphene bilayers are found to have Bernal stacking (as in their parent material graphite). Labeling the layers as left (L) and right (R), the Bernal structure has atoms of one sublattice in the left layer (AL) adjacent to atoms of the other sublattice in the right layer (BR) so that these are tunnel coupled, while the other two atoms in the unit cell [left layer, B sublattice (BL) and right layer, A sublattice (AR)] have no interlayer coupling. In this configuration, the energy varies quadratically about the Dirac points. The large density of states associated with this leads to broken-symmetry ground states even for an infinitesimal electron-electron interaction. Many such states have been proposed for the system,^{8–20} and some transport experiments suggest a gap opening in the spectrum^{21–24} as is expected in many of these scenarios.

Other stackings for bilayer graphene are possible. Recently, AA-stacked bilayers have been identified experimentally²⁵ in which all atoms of one layer are directly adjacent, and tunnel coupled, to the equivalent atoms in the other layer. This type of stacking also occurs locally in large regions of small angle twisted bilayers.^{26,27} The focus of our study

will be on the electronic states of such AA-stacked graphene bilayers.

When interactions are ignored, the system may be conveniently represented in terms of bonding and antibonding states, each separately supporting its own Dirac spectrum, with the Dirac points separated in energy by $2t_1$, with t_1 the interlayer hopping parameter. At half-filling, the Fermi surface coincides with the circle in momentum space where these spectra cross. When interactions are introduced, this spectrum becomes unstable to the opening of a gap due to the perfect nesting of the Fermi surfaces in the two bands. This situation is analogous to what occurs in double-layer graphene separated by a thin insulating barrier, in which tunneling between layers is suppressed but interlayer interactions are not. It is widely believed that a gap opens in the spectrum in this system, with the ground state forming an interlayer exciton condensate.^{28–31} In the limit of vanishing interlayer separation d , the two systems indeed are isomorphic.

When d is nonvanishing, the double-layer graphene system and the AA-stacked bilayer differ in an important, qualitative way. The double-layer Hamiltonian has $U(1)$ symmetry, which is broken in the ground state, whereas, as explained below, the AA bilayer system has only a Z_2 (Ising) symmetry, which is also broken in the ground state. In what follows, we compute the band structure of this system in the Hartree-Fock approximation, demonstrating a gap opening associated with the broken symmetry. This gap serves as an estimate of the mean-field transition temperature. To take into account the subtle effects of screening, we include a static dielectric constant in the effective electron-electron interaction, which is computed self-consistently in the presence of the gap in the energy spectrum.³¹ For typical values of the system parameters, the resulting gap is of order 5 meV, suggesting a mean-field ordering temperature of 50 K. In the broken symmetry state, we find a staggered charge density distribution such that charge is transferred between layers, but in opposite directions for each of the sublattices. Although our calculations do not include spin explicitly, it is likely that this charge density wave ordering would be compensated by the two spin species, yielding antiferromagnetic spin ordering in the system.³²

In two dimensions, the mean-field transition temperature greatly overestimates the true disordering T_c by missing the low-energy collective excitations as well as crucial topological excitations. In the limit $d \rightarrow 0$, where the system has $U(1)$ symmetry, the latter are vortices, and the disordering transition should be in the Kosterlitz-Thouless (KT) universality class.³³ In this case, the transition temperature is controlled by the phase stiffness of the $U(1)$ degree of freedom. This stiffness is challenging to compute accurately because it depends exponentially on the effective interaction strength, so that different assumptions about screening lead to vastly different estimates of the critical temperature.^{28,30,31,34,35} For $d > 0$, the disordering transition falls into the Ising universality class, and may be understood as being driven by a proliferation of domain walls.³³ Despite the difference from the KT transition, we argue below that the transition is still controlled by the effective phase stiffness, and that, in principle, the Ising transition would continuously go into the KT transition if the layer spacing d could be continuously tuned to zero. Combining this analysis with a calculation of the phase stiffness using the self-consistently screened interaction, we arrive at an estimate of T_c of order 3 K for the AA-stacked graphene bilayer.

In principle, the Ising transition that we analyze in this work should present itself as singularities in thermodynamic quantities of the system. These would be considerably less subtle than what is expected for the KT transition associated with the related double-layer system. More directly, the symmetry breaking in the ground state should be visible at low temperature in STM experiments with sufficient resolution to distinguish the two sublattices.

This article is organized as follows. In Sec. II, we describe the model used to describe the system, a single Dirac cone treated in a continuum approximation. In Sec. III, we describe the broken symmetry state within the Hartree-Fock approximation, including the self-consistent approach to the screening of the interactions. Section IV describes a simple continuum model of the energetics of the order parameter, how this leads to an Ising transition controlled by the phase stiffness in the energy functional, and the resulting estimate of the disordering temperature. We conclude in Sec. V with a summary of our results. Appendix provides details of how screening is incorporated into our calculation.

II. MODEL

We consider a single-valley model for electrons in graphene in the continuum limit. Near the Dirac point, the noninteracting Hamiltonian takes the form³⁶

$$H_0 = \hbar v_F \sum_{\mathbf{k}, i=L,R} (k_x - i k_y) c_{A\mathbf{k}}^\dagger c_{B\mathbf{k}} - t_1 \sum_{\mathbf{k}, \alpha=A,B} c_{\alpha\mathbf{k}}^\dagger c_{\alpha\mathbf{k}} + \text{H.c.}, \quad (1)$$

where the operator $c_{\alpha\mathbf{k}}^\dagger$ creates an electron on sublattice α in layer i with momentum \mathbf{k} . The interlayer hopping matrix element is t_1 , which is estimated to have values of order $\sim 0.12t$,⁷ where t is the nearest-neighbor intralayer hopping parameter. In the continuum limit, t enters only through the electron speed $\hbar v_F = \frac{\sqrt{3}}{2}ta$, where a is the monolayer graphene lattice parameter. Valley and spin degrees

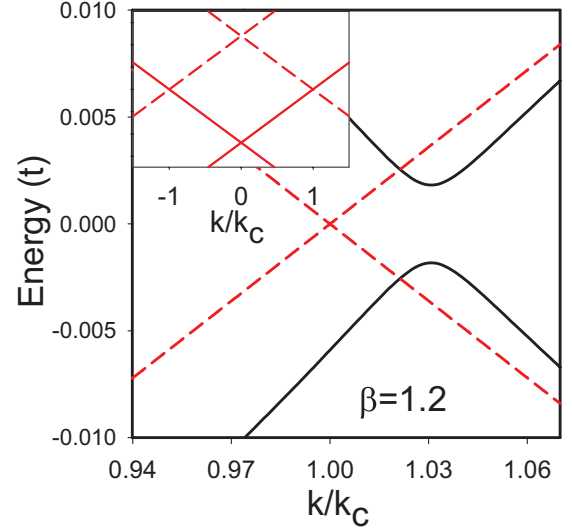


FIG. 1. (Color online) Energy spectrum for AA-stacked bilayer graphene. Solid lines correspond to the Hartree-Fock energy bands for $\beta = 1.2$ near k_c . Dashed lines are single-electron energies in the absence of interactions. (Inset) Noninteracting single-electron energies over a broader momentum range. Solid (dashed) lines represent bonding (antibonding) states.

of freedom are not explicitly treated. The eigenvalues of H_0 are $\varepsilon(k) \pm t_1$, and represent bonding (−) and antibonding (+) linear combinations of left and right layer wave functions. The monolayer graphene dispersion is $\varepsilon(k) = \hbar v_F k$, where $s = -1$ indicates an electron-like band and $s = +1$ a holelike band.

The inset of Fig. 1 illustrates the one-electron band structure as a function of the momentum near a Dirac point. The result is highly analogous to what one finds in the biased double-layer case.^{28–30} As in that case, when the system is neutral, the Fermi surface corresponds with the circle of radius $k_c = t_1/\hbar v_F$ at which the holelike antibonding band spectrum crosses the electron-like bonding band spectrum. Because of this perfect nesting, the system is unstable to the formation of a particle-hole pair condensate^{37,38} when interactions are included.

We model the interaction part of the Hamiltonian as

$$H_{ee} = \frac{1}{2S} \sum_{\alpha, \beta} \sum_{i, j} \sum_{\mathbf{q}, \mathbf{k}, \mathbf{k}'} : c_{\alpha i \mathbf{k}}^\dagger c_{\alpha i \mathbf{k} - \mathbf{q}} V^{ij}(\mathbf{q}) c_{\beta j \mathbf{k}'}^\dagger c_{\beta j \mathbf{k}' + \mathbf{q}} : , \quad (2)$$

where S is the sample area, $V^{LL}(\mathbf{q}) = V^{RR}(\mathbf{q})$ and $V^{LR}(\mathbf{q}) = V^{RL}(\mathbf{q})$ are Fourier transforms of screened intra and interlayer electron-electron interactions, respectively, and $: \dots :$ indicates normal ordering. Equation (2) assumes that the interactions preserve the sublattice and valley indices.³

Because of the perfect nesting of the Fermi surfaces in the bonding/antibonding bands, we expect that electron-electron interactions drive an instability involving the mixing of these bands near the Fermi circle at k_c . Within the Hartree-Fock approximation, this is expressed as a condensation of electron-hole pairs. Any estimate of the electron-hole pairing amplitude depends sensitively on the level of screening included in the model. Because of the long-range character of the Coulomb interaction, an unscreened electron-electron interaction results

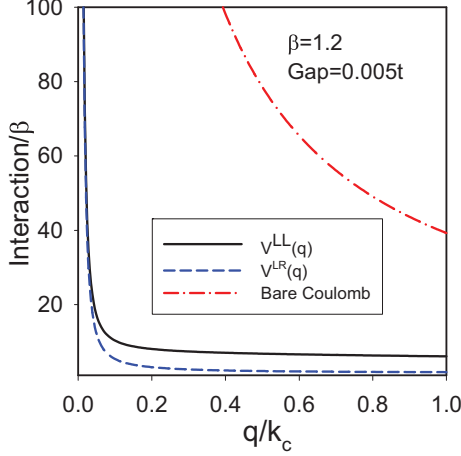


FIG. 2. (Color online) Inter and intralayer interactions as a function of q for a condensate with $\beta = 1.2$ and gap $E_g = 0.005t$. For comparison, the bare Coulomb interaction is also shown.

in very large gaps in the spectrum, and in a high critical temperature.^{28,29} To go beyond this, one may incorporate screening via a dielectric function appropriate for metallic graphene, completely eliminating the effective long-range nature of the interaction. This results in both a very small gap and a very low critical temperature.^{30,39,40} In this work, we adopt a model of static screening⁴¹ that allows for its suppression at large distances, due to the appearance of the gap in the spectrum due to electron-hole condensation. The gap and dielectric screening functions are computed in a self-consistent way.^{31,34,35} In Appendix, we provide some details of the polarization function matrix and how this leads to our model of the screened potential.

In Fig. 2, we plot a typical result for the inter and intralayer interactions for a condensate with an assumed gap $E_g = 0.005t$. At large q , the interactions are highly reduced from the bare Coulomb interaction. However, for values of q below $\sim E_g/\hbar v_F$, $V^{LL}(q)$ and $V^{LR}(q)$ are not fully screened, and one finds a Coulomb-like $1/q$ divergence. This model thus produces an intermediate behavior between approaches using unscreened and metallically screened interactions. A complication of this approach is that it requires knowledge of the single-particle band structure, so that the screened interactions must be computed self-consistently with states and energies found in the Hartree-Fock approximation. We next turn to a discussion of this calculation.

III. HARTREE-FOCK APPROXIMATION

In the Hartree-Fock (HF) approximation, the electron-electron interaction is replaced in the Hamiltonian by

$$H_{ee}^{\text{HF}} = -\frac{1}{S} \sum c_{\alpha i \mathbf{k}}^\dagger c_{\beta j \mathbf{k}} V^{ij}(|\mathbf{k} - \mathbf{k}'|) \langle c_{\alpha j \mathbf{k}'}^\dagger c_{\alpha i \mathbf{k}'} \rangle. \quad (3)$$

The energy of the ground state can be lowered by opening a gap at the crossing between the electron-like band of the bonding energy states and the holelike band of the antibonding spectrum. To do this, we consider broken symmetry states characterized by the circularly symmetric order

parameters:

$$\begin{aligned} A(k) + iB(k) &= \langle c_{\text{ARk}}^\dagger c_{\text{ALk}} \rangle = \langle c_{\text{BRk}}^\dagger c_{\text{BLk}} \rangle^* \quad \text{and} \\ Q(k) &= \langle c_{\text{ARk}}^\dagger c_{\text{ARk}} \rangle = \langle c_{\text{BLk}}^\dagger c_{\text{BLk}} \rangle \\ &= 1 - \langle c_{\text{BRk}}^\dagger c_{\text{BRk}} \rangle = 1 - \langle c_{\text{ALk}}^\dagger c_{\text{ALk}} \rangle. \end{aligned} \quad (4)$$

These forms are valid provided one assumes the electron-like antibonding band is completely empty, and the holelike bonding band is completely full. These assumptions are sensible because neither of these bands approach the Fermi energy in the noninteracting state. The self-energies associated with these parameters are

$$\begin{aligned} \Delta_R^{\text{LR}}(k) + i\Delta_I^{\text{LR}}(k) &= -\frac{1}{S} \sum_{\mathbf{k}'} V^{\text{LR}}(|\mathbf{k} - \mathbf{k}'|) [A(k) + iB(k)], \\ \Delta^{\text{LL}}(k) &= -\frac{1}{S} \sum_{\mathbf{k}'} V^{\text{LL}}(|\mathbf{k} - \mathbf{k}'|) \left[Q(k) - \frac{1}{2} \right], \\ \Delta^{\text{RR}}(k) &= -\frac{1}{S} \sum_{\mathbf{k}'} V^{\text{RR}}(|\mathbf{k} - \mathbf{k}'|) \left[Q(k) - \frac{1}{2} \right]. \end{aligned} \quad (5)$$

Rewriting Eq. (3) in terms of these quantities, the resulting HF Hamiltonian may be diagonalized, yielding eigenenergies $\pm \varepsilon_\pm(k)$ of the form

$$\varepsilon_\pm(k) = \sqrt{\{\hbar v_F k \mp [t_1 + \Delta_R^{\text{LR}}(k)]\}^2 + [\Delta_I^{\text{LR}}(k) + \Delta^{\text{LL}}(k)]^2}. \quad (6)$$

In terms of the self-energies and eigenenergies, at finite temperature, the order parameters take the forms

$$\begin{aligned} A(k) + iB(k) &= \frac{1}{4} \left\{ \frac{-\hbar v_F k + t_1 - \Delta_R^{\text{LR}}(k) + i\Delta_I^{\text{LR}}(k)}{\varepsilon_-} \tanh \left[\frac{\varepsilon_-(k)}{2k_B T} \right] \right. \\ &\quad \left. + \frac{\hbar v_F k + t_1 - \Delta_R^{\text{LR}}(k) + i\Delta_I^{\text{LR}}(k)}{\varepsilon_+} \tanh \left[\frac{\varepsilon_+(k)}{2k_B T} \right] \right\}, \end{aligned} \quad (7)$$

$$Q(k) = \frac{1}{2} - \frac{\Delta^{\text{LL}}(k)}{4} \left\{ \frac{\tanh \left[\frac{\varepsilon_-(k)}{2k_B T} \right]}{\varepsilon_-(k)} + \frac{\tanh \left[\frac{\varepsilon_+(k)}{2k_B T} \right]}{\varepsilon_+(k)} \right\}. \quad (8)$$

In Figs. 1 and 3, we plot the band structure and the order parameters obtained from self-consistently solving Eqs. (4)–(8) for $\beta = 1.2$. As expected, the coherence between the bonding and antibonding bands opens a gap near k_c . Moreover, the minimum gap occurs at larger momentum than k_c because the self-energy Δ_R^{LR} acts as an extra contribution to the hopping parameter connecting the layers.

The inset of Fig. 4 illustrates the value of the gap as a function of the strength of the Coulomb interaction β . In this example, we adopted a hopping matrix element $t \sim 2.8$ eV. A moderate value of $\beta \sim 0.6$ corresponds to a background dielectric constant of ~ 3.7 , which could for example be provided by a SiO₂ substrate. At this value of β one finds $E_g \sim 5.6$ meV, suggesting a mean-field transition temperature of several tens of degrees Kelvin. However, as we discuss below, fluctuations will considerably reduce the critical temperature.

The ordering in this system arises from spontaneous coherence between independent bands. For momenta $k \ll k_c$,

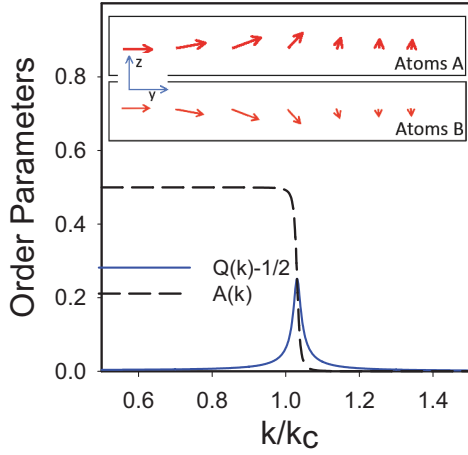


FIG. 3. (Color online) Order parameters as a function of k for $\beta = 1.2$. (Inset) Schematic plot of the direction and magnitude of the isospin on atoms A and B as a function of momentum.

the two occupied bands have a bonding character and $A(k) \approx 1/2$. For values of $k \gg k_c$, the holelike antibonding band and the electron-like bonding band are occupied, and $A(k) \approx 0$. In these two limits, $Q(k)$ is close to its noninteracting value, $Q(k) \sim 1/2$, because the large energy differences between states in different bands allows for little admixture between them in the HF state. For values of $k \sim k_c$, the similarity in energy of bonding and antibonding states allows them to admix and thereby lower the energy of the system. It is in this range that $Q(k)$ significantly differs from its noninteracting value, so that we can use this quantity as a measure of the anomalous order in the HF state.

A physical picture of the ordering can be found in the language of quantum ferromagnetism. We define an isospin degree of freedom for each of the sublattices, in which spin “up” corresponds to an electron in the left layer, and spin “down” indicates an electron residing in the right layer. Assuming we consider only states in which the holelike bonding band is completely full, and the electron-like antibonding band

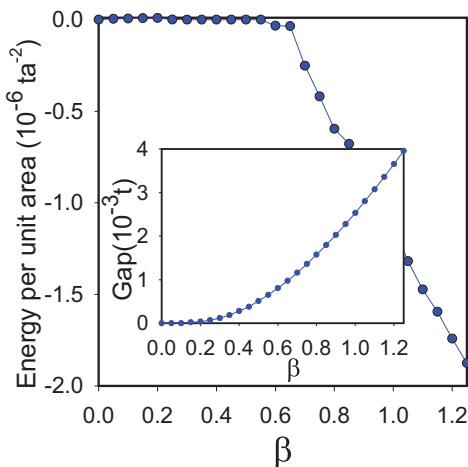


FIG. 4. (Color online) Difference in energy per unit area, as a function of the strength of the electron-electron interaction, between the Ising and the U(1) phases (see text). (Inset) Gap as a function of β .

is completely empty, one may easily confirm that the isospin expectation values in the HF state can be written in terms of spin vectors for each sublattice, satisfying

$$\begin{aligned} S_{x,A}(k) &= S_{x,B}(k) = 2A(k), \\ S_{y,A}(k) &= -S_{y,B}(k) = 2B(k), \\ S_{z,A}(k) &= -S_{z,B}(k) = 2Q(k) - 1. \end{aligned} \quad (9)$$

Note that because of the background filled holelike bonding band, these vectors are not constant in magnitude. However, they *can* be written in terms of a vector field of fixed magnitude $\vec{\sigma}(k)$ with constant vectors in the \hat{x} direction subtracted (added) for the A (B) sublattice.

In the noninteracting state, one finds that S_x for both sublattices takes on its maximal value for $k < k_c$, and $S_{(y,z)}$ both vanish. As k increases through k_c , there is a sudden change in which \vec{S} collapses to zero. The introduction of the nonvanishing Q order parameter allows \vec{S} to evolve *continuously* from its small k value to zero at large k , lowering the isospin exchange energy and thus the total energy of the state.⁴² This behavior is illustrated in Fig. 3. In this evolution, $\vec{\sigma}$ rotates through the \hat{y} direction with no component in the \hat{z} direction, because tilting in the latter direction amounts to a charge imbalance between the layers, adding a positive charging (Hartree) energy to the total ground-state energy.⁴³ Note that in the limit $d \rightarrow 0$, this latter energy cost vanishes, so that the rotation can be through any direction in the $\hat{y} - \hat{z}$ plane with no additional energy cost, and the ground state has a broken U(1) symmetry. For nonvanishing d , the only choice that does not affect the energy of the state is whether the rotation occurs through the positive or negative \hat{y} direction. One thus obtains a broken Z_2 symmetry in the ground state.

Physically, this broken symmetry manifests itself as a transfer of charge between the layers, in opposite directions for the two sublattices. A related ordering for this system has recently been suggested in a tight-binding Hubbard model.³² Were spin to be included in our model, we expect that the spontaneous orderings for opposing spin directions would be staggered, yielding the essentially the same antiferromagnetic ordering in our system that is found in the tight-binding Hubbard model. We note that the very short-range interaction employed in a Hubbard model implies strong screening, which is not consistent with the gap opening in the spectrum. Our calculation strongly suggests that the antiferromagnetic ordering will still be present when the long-range nature of the Coulomb interaction is included.

IV. FINITE TEMPERATURE ISING TRANSITION

In AA-stacked bilayer graphene, the distance between layers is relatively small ($d = 1.2a$, with a the graphene lattice constant). Moreover, screening is very efficient in this system at large q . In the range of wave vectors relevant for the formation of the condensate ($k \sim k_c$), these two effects lead to intra and interlayer electron-electron interactions, which are very similar, as illustrated in Fig. 2. Because of this, the difference in energy between a phase with U(1) symmetry obtained by taking $V^{\text{LL}}(q) = V^{\text{LR}}(q)$, and one with broken Ising symmetry, from a Hamiltonian in which the difference between the intra and interlayer interactions is retained, is very small. This is

illustrated in Fig. 4. It is then interesting to consider how the KT transition expected in the $d \rightarrow 0$ limit is related to the Ising transition expected for the $d > 0$ case. In this section, we argue that the transitions are continuously connected, based on a scaling argument and that both transition temperatures are set by the effective phase stiffness of the system.

To address this issue, we consider an effective low-energy functional of the form

$$E = \int d\mathbf{r} \left\{ \frac{\rho_s}{2} |\vec{\nabla}\theta(\mathbf{r})|^2 - h \cos[2\theta(\mathbf{r})] \right\}, \quad (10)$$

where θ is a phase angle for the electron-hole condensate, which can be interpreted as the angle in the \hat{y} - \hat{z} plane made the vectors \vec{S}_α described in the last section, h is the charging energy cost for $d > 0$, which vanishes as $d \rightarrow 0$, and ρ_s is the phase stiffness of the U(1) degree of freedom. For $h = 0$, the quantity ρ_s may be estimated by⁴⁴

$$\rho_s(T) = \frac{t_1}{4} k_B T \sum_{n=-\infty}^{n=\infty} \frac{E_{g,0}^2(T)}{[\pi k_B T (2n+1)]^2 + E_{g,0}^2(T)}^{3/2}, \quad (11)$$

where $E_{g,0}$ is the energy gap when $d = 0$, which is somewhat smaller than E_g .

Equation (10) may be placed on a lattice to allow for the possibility of vortex excitations. For $h = 0$, the Hamiltonian then has the form $H_{XY} = -J \sum_{\langle ij \rangle} \cos[\theta_i - \theta_j]$, where θ_i is a phase angle at site i , which is assumed to be on a square lattice, the sum is over nearest neighbors sites, and $J \approx \rho_s$. This is just the XY model, and it supports a KT transition at $T_{KT} = 0.89J$.⁴⁵ Equation (10) for $h = 0$ and H_{XY} share the same U(1) symmetry, and provided one allows for vortex configurations in the former, both models support a KT transition.

This observation is dramatically changed when $h > 0$, which introduces a perturbation in the U(1) theory that is relevant for any temperature below T_{KT} .⁴⁶ The usual interpretation of this behavior is that the KT transition is eliminated,^{47,48} and the only thermodynamic phase transition remaining is of the Ising type. In applying Eq. (10) to the AA bilayer graphene problem, the smallness of the effective h , which vanishes in the $d \rightarrow 0$ limit, naïvely suggests a very small T_c associated with this Ising transition. With $T_{KT} \sim \rho_s$, if this is so then it is unclear what becomes of the KT transition as soon as h is raised from zero.

To address these questions, we first consider how to construct an Ising model that appropriately describes Eq. (10) as the Ising transition is approached. This can be accomplished by noting that the Ising transition may be interpreted as a proliferation of domain walls,³³ so that one should match the energy cost of overturned neighboring Ising spins σ_z in the Ising Hamiltonian $H_{\text{Ising}} = -K \sum_{\langle ij \rangle} \sigma_z(i) \sigma_z(j)$ with the energy of a domain wall (DW) in Eq. (10). Moreover, the nearest-neighbor distance in H_{Ising} should be taken as the DW width of Eq. (10). The DW configuration of Eq. (10) may be explicitly computed with standard methods,³³ yielding the form

$$\theta(x) = \pm 2 \arctan[\exp(x/\xi)],$$

with an energy per unit length $\varepsilon_{\text{DW}} = 4\sqrt{\rho_s h}$ and DW width $\xi = \sqrt{\rho_s/h}/2$. Identifying this last quantity with the lattice constant of H_{Ising} , we arrive at the estimate

$2K = \varepsilon_{\text{DW}} \xi = 2\rho_s$. Using the two-dimensional DW proliferation transition temperature³³ $k_B T_{\text{DW}} = 2K / \ln(2.63)$, we arrive at an estimate for the Ising transition in the bilayer system of $k_B T_{\text{Ising}} = 2\rho_s / \ln(2.63)$.

Remarkably, h does not explicitly enter into this result, so that the transition temperature does *not* vanish as $h \rightarrow 0$. Physically, this can be understood by recognizing that for small h , the unit cell area ξ^2 of H_{Ising} encompasses an increasingly large physical area of the system as $h \rightarrow 0$, such that the energy to overturn θ over this length scale remains finite even as the microscopic energy cost to do so vanishes. It is interesting to note that our estimate of $k_B T_{\text{Ising}}$, like $k_B T_{\text{KT}}$, depends only on ρ_s , and in fact *exceeds* the standard KT transition temperature, which in the simplest estimate³³ is given by $k_B T_{\text{KT}} = \frac{\pi}{2} \rho_s$. We are then left with the question of how the Ising transition vanishes and the KT transition emerges as $h \rightarrow 0$.

The key to answering this question is to note that the two transitions involve the proliferation of topologically distinct defects, so that relating them requires a model that has both of them. A simple way to do this is to assume that the perturbation h may be ignored below the scale ξ , so that ρ_s is renormalized by vortices in just the way it would in the absence of the U(1) symmetry-breaking term; above this scale, we assume the vortices are linearly confined into vortex-antivortex pairs,⁴⁹ and can be ignored at such long length scales.⁵⁰

To carry this out, we use the renormalization group (RG) flow equations for the KT transition, which have the well-known form:⁴⁷

$$\frac{d\tilde{\rho}_s^{-1}}{d\ell} = 4\pi^2 y^2, \quad (12)$$

$$\frac{dy}{d\ell} = (2 - \pi \tilde{\rho}_s) y, \quad (13)$$

where y is the vortex fugacity, assumed to be small, $\tilde{\rho}_s = \rho_s / k_B T$, and ℓ characterizes the multiplicative rescaling factor of the shortest length scale in the effective Hamiltonian, $a \rightarrow ae^\ell$. We assume the ultimate scale for this microscopic length scale is ξ , which is connected to the phase stiffness by $\tilde{\rho}_s = (h/k_B T) \xi^2$.

Figure 5 illustrates this relation between (the renormalized) $\tilde{\rho}_s$ and ξ , along with the RG flows for different initial values

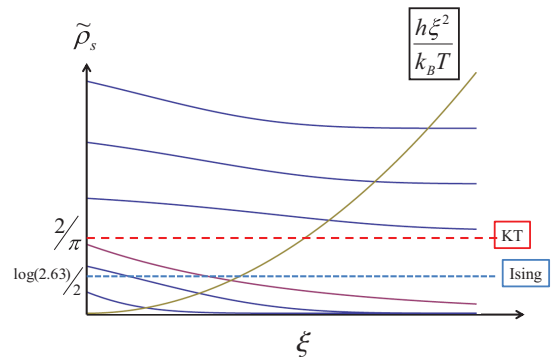


FIG. 5. (Color online) Schematic RG flows of $\tilde{\rho}_s$ as a function of scale size ξ . Flow stops when $\tilde{\rho}_s(\xi)$ matches $h\xi^2/k_B T$. This value sets the exchange energy for an effective Ising model. Dotted (blue) line indicates critical value for Ising transition. Dashed (red) line indicates critical value for KT transition.

of $\tilde{\rho}_s$. For simplicity, we ignore the renormalizations of y and h —including these would not alter the qualitative physics. The initial value of $\tilde{\rho}_s$ [from Eq. (10)] sets the value on the farthest left of the flow, and as can be seen in the figure, $\tilde{\rho}_s$ is always renormalized downward. Following the logic described above, the value of K used in the effective Ising model should be taken as $K = k_B T \tilde{\rho}_s(\xi)$, with ξ satisfying the self-consistency condition $\tilde{\rho}_s(\xi) = h \xi^2 / k_B T$.

The KT RG flows have a well-known property that in the limit $\xi \rightarrow \infty$, $\tilde{\rho}_s$ jumps from $2/\pi$ to zero as T passes from below to above T_{KT} . We illustrate this critical value as a dashed line in Fig. 5. Assuming the Ising transition occurs, as remarked above, at a higher transition temperature than the KT transition for $h = 0$, the critical $\tilde{\rho}_s$ at which the Ising transition occurs is below the critical value for the KT transition. This is illustrated as dotted line in Fig. 5. One can now see how h controls the Ising transition. For relatively large h , $h \xi^2 / k_B T$ will curve sharply upward, and $\tilde{\rho}_s$ will undergo only a small downward renormalization, and we expect $k_B T_{\text{Ising}} \approx \frac{2\rho_s}{\ln(2.63)} = 2.07\rho_s$, with ρ_s close to the initial value appearing in Eq. (10). As h decreases, the downward renormalization of $\tilde{\rho}_s$ becomes increasingly pronounced, lowering the critical temperature for the Ising transition. In the limit $h \rightarrow 0$, $\tilde{\rho}_s$ either flows to a value above $2/\pi$, which is above the dotted line (indicating an ordered Ising state), or flows to zero, below the dotted line (indicating a disordered Ising state.) In this way, the Ising transition continuously flows into the KT transition in the limit $h \rightarrow 0$.⁵¹ This indicates that, in an h - T phase diagram, the transition will be in the Ising universality class for any nonvanishing h , but at the endpoint $h = 0$, the transition will be in the KT universality class.

In Fig. 6, we illustrate an estimate of the critical Ising temperature for the AA bilayer graphene system when vortices are ignored. In this situation the mean-field $\rho_s(T)$ may be computed from Eq. (11); the Ising transition will then approximately occur at the temperature where this coincides with $\rho_s(T) = k_B T / 2.07$. Figure 6(a) illustrates this matching condition, and Fig. 6(b) illustrates the resulting transition temperature as a function of the electron-electron interaction strength β . For $\beta \approx 0.6$, we arrive at an estimate of $T_c \approx 10^{-4} t / k_B \sim 3$ K.

V. SUMMARY AND DISCUSSION

In this work, we have considered broken symmetry states of AA-stacked bilayer graphene. Due to the interlayer tunneling, this system has two Dirac cones symmetrically displaced above and below zero energy, so that at zero doping and in the absence of interactions, there is a band crossing precisely at the Fermi circle. This perfect nesting leads to an instability in the presence of arbitrarily small interaction strength, in which a gap opens around the Fermi energy. This gap arises from spontaneous coherence between the bonding and antibonding bands, in a manner analogous to what happens in double-layer graphene systems with an interlayer bias. This spontaneous coherence leads to a transfer of charge from one layer to the other, in opposite directions for the two sublattices so there is no net charge imbalance between layers.

Unlike the double-layer case, the difference between inter and intralayer interactions in the AA-stacked bilayer leads to

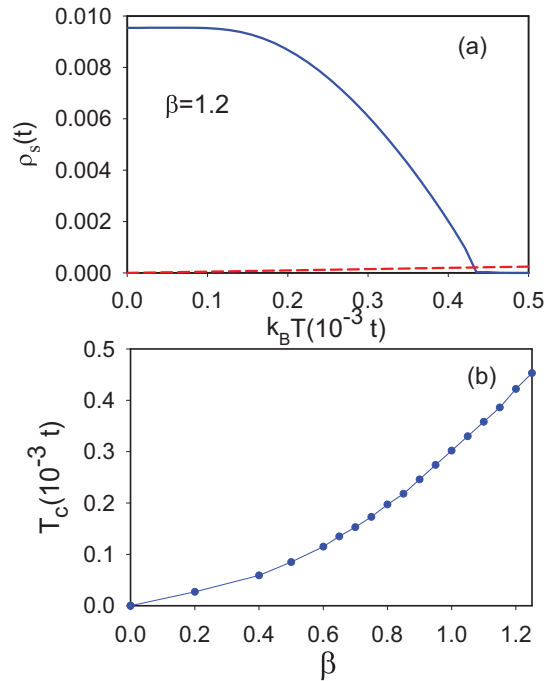


FIG. 6. (Color online) (a) Graphical solution of equation $k_B T_{\text{Ising}} \approx 2.07\rho_s$ for the critical temperature. Continuous line corresponds to $\rho_s(T)$ and the red dashed line is a straight line of slope 2.07. (b) Values of the critical temperature as function of the strength of the electron-electron interaction.

an Ising-like order parameter, rather than one with an XY character. We argued that the Ising transition in the former case and KT transition in the latter are continuously connected as the layer spacing d vanishes (eliminating the difference between the two types of interactions.) Both transitions are controlled by the effective (iso-)spin stiffness of the system. A calculation of this, including screening which self-consistently incorporates the effect of the gap, yields a critical temperature estimate of a few degrees Kelvin.

Our analysis neglects the presence of multiple Dirac points of the single-layer system, which will be present due to valley and spin degeneracy. Incorporation of this effect is likely to yield multiple copies of the order parameter in the system, which could then be interdigitated in such a way as to cancel out the opposing interlayer charge polarization we find for the different sublattices. Within our continuum model, it is not obvious whether this would occur via the spin or valley degree of freedom. However, we believe that when the microscopic spatial separation of the two sublattices is taken into account, it is more likely that this would occur through the spin degree of freedom since the microscopic charge modulation could be canceled in more detail. The resulting ground state would have antiferromagnetic order.³²

In principle, the staggered ground-state ordering could be detected by spin-polarized tunneling into one of the two sides of the structure. It is also interesting to note that thermodynamic measurements could, in principle, show signs of the expected Ising transition, for example, in singular behavior of the heat capacity. Such thermodynamic singularities are considerably more accessible in this system than in the double-layer system because disordering in the latter occurs

through a KT transition, which is considerably more subtle than the Ising transition.

ACKNOWLEDGMENTS

The authors would like to thank Ganpathy Murthy for enlightening discussions on the connection between the Ising and Kosterlitz-Thouless transitions. Funding for the work described here was provided by MICINN-Spain via grants FIS2012-33521 (LB) and by the NSF through Grant No. DMR-1005035 (HAF).

APPENDIX: DIELECTRIC CONSTANT AND SCREENED INTERACTION

We define the polarizabilities

$$\Pi_{\alpha,\beta}(q,\omega) = -\frac{g_s g_v}{S} \sum_{\mathbf{k},s,s'} \frac{n_{s,\mathbf{k}} - n_{s',\mathbf{k}'}}{\omega + \varepsilon_{s,\mathbf{k}} - \varepsilon_{s',\mathbf{k}'}} F_{s,s'}^{\alpha,\beta}(\mathbf{k},\mathbf{k}'), \quad (\text{A1})$$

where $\mathbf{k}' = \mathbf{k} + \mathbf{q}$, $g_s = 2$ and $g_v = 2$ are the spin and valley degeneracies, S is the sample area and $\varepsilon_{s,\mathbf{k}}$ are the eigenvalues of the band s with wave vector \mathbf{k} . The indices α and β are the layer indices. The couplings F have the form

$$F_{s,s'}^{\alpha,\beta}(\mathbf{k},\mathbf{k}') = \langle s,\mathbf{k} | P_\alpha | s',\mathbf{k}' \rangle \langle s',\mathbf{k}' | P_\beta | s,\mathbf{k} \rangle, \quad (\text{A2})$$

where P_α is a layer projection operator,

$$P_L = \begin{pmatrix} 1 & 0 & 0 & 0 \\ 0 & 1 & 0 & 0 \\ 0 & 0 & 0 & 0 \\ 0 & 0 & 0 & 0 \end{pmatrix} \text{ and } P_R = \begin{pmatrix} 0 & 0 & 0 & 0 \\ 0 & 0 & 0 & 0 \\ 0 & 0 & 1 & 0 \\ 0 & 0 & 0 & 1 \end{pmatrix}. \quad (\text{A3})$$

These operators are written in the basis LA, LB, RA, RB. Equation (A1) depends on both the eigenvalues and eigenvectors of the HF Hamiltonian, which in turn depends on the order parameters characterizing the condensate. By symmetry, $\Pi_{LL} = \Pi_{RR}$ and $\Pi_{LR} = \Pi_{RL}$.

Using these polarizabilities, we obtain effective intra and interlayer interactions in the RPA:

$$\begin{pmatrix} V_{LL}(q) & V_{LR}(q) \\ V_{LR}(q) & V_{LL}(q) \end{pmatrix} = v(q) \left[\begin{pmatrix} 1 & 0 \\ 0 & 1 \end{pmatrix} + v(q) \begin{pmatrix} 1 & e^{-qd} \\ e^{-qd} & 1 \end{pmatrix} \begin{pmatrix} \Pi_{LL}(q) & \Pi_{LR}(q) \\ \Pi_{LR}(q) & \Pi_{LL}(q) \end{pmatrix} \right]^{-1} \begin{pmatrix} 1 & e^{-qd} \\ e^{-qd} & 1 \end{pmatrix}, \quad (\text{A4})$$

where d is the distance between layers. From this equation, we finally obtain

$$V_{LL}(q) = v(q) \frac{1 + v(q)\Pi_{LL}(q)(1 - e^{-2qd})}{[1 + v(q)\Pi_{LL}(q) + v(q)\Pi_{LR}(q)e^{-qd}]^2 - [v(q)\Pi_{LR}(q) + v(q)e^{-qd}\Pi_{LL}(q)]^2}, \quad (\text{A5})$$

$$V_{LR}(q) = v(q) \frac{e^{-qd} + v(q)\Pi_{LR}(q)(e^{-2qd} - 1)}{[1 + v(q)\Pi_{LL}(q) + v(q)\Pi_{LR}(q)e^{-qd}]^2 - [v(q)\Pi_{LR}(q) + v(q)e^{-qd}\Pi_{LL}(q)]^2}.$$

¹A. H. Castro-Neto, F. Guinea, N. M. R. Peres, K. S. Novoselov, and A. K. Geim, *Rev. Mod. Phys.* **81**, 109 (2009).

²J. Gonzalez, F. Guinea, and M. Vozmediano, *Nuc. Phys. B* **424**, 593 (1994).

³V. N. Kotov, B. Uchoa, V. M. Pereira, F. Guinea, and A. H. Castro Neto, *Rev. Mod. Phys.* **84**, 1067 (2012).

⁴J. E. Drut and T. A. Lähde, *Phys. Rev. Lett.* **102**, 026802 (2009).

⁵J. Wang, H. A. Fertig, and G. Murthy, *Phys. Rev. Lett.* **104**, 186401 (2010).

⁶J. Wang, H. A. Fertig, G. Murthy, and L. Brey, *Phys. Rev. B* **83**, 035404 (2011).

⁷E. McCann and M. Koshino, *arXiv:1205.6953* [cond-mat.mes-hall].

⁸R. Nandkishore and L. Levitov, *Phys. Rev. B* **82**, 115124 (2010).

⁹F. Zhang, J. Jung, G. A. Fiete, Q. Niu, and A. H. MacDonald, *Phys. Rev. Lett.* **106**, 156801 (2011).

¹⁰J. Jung, F. Zhang, and A. H. MacDonald, *Phys. Rev. B* **83**, 115408 (2011).

¹¹F. Zhang, H. Min, M. Polini, and A. H. MacDonald, *Phys. Rev. B* **81**, 041402 (2010).

¹²O. Vafek and K. Yang, *Phys. Rev. B* **81**, 041401 (2010).

¹³Y. Lemonik, I. L. Aleiner, C. Toke, and V. I. Fal'ko, *Phys. Rev. B* **82**, 201408 (2010).

¹⁴E. V. Castro, N. M. R. Peres, T. Stauber, and N. A. P. Silva, *Phys. Rev. Lett.* **100**, 186803 (2008).

¹⁵O. Vafek, *Phys. Rev. B* **82**, 205106 (2010).

¹⁶F. Zhang and A. H. MacDonald, *Phys. Rev. Lett.* **108**, 186804 (2012).

¹⁷M. Kharitonov, *Phys. Rev. B* **86**, 195435 (2012).

¹⁸R. E. Throckmorton and O. Vafek, *Phys. Rev. B* **86**, 115447 (2012).

¹⁹V. Cvetkovic, R. E. Throckmorton, and O. Vafek, *Phys. Rev. B* **86**, 075467 (2012).

²⁰L. Zhu, V. Aji, and C. M. Varma, *Phys. Rev. B* **87**, 035427 (2013).

²¹J. Velasco, L. Jing, W. Bao, Y. Lee, P. Kratz, V. Aji, M. Bockrath, C. N. Lau, C. Varma, R. Stillwell, D. Smirnov, F. Zhang, J. Jung, and A. H. MacDonald, *Nat. Nanotechnology* **7**, 156 (2012).

²²R. T. Weitz, M. T. Allen, B. E. Feldman, J. Martin, and A. Yacoby, *Science* **330**, 812 (2010).

²³W. Bao, J. Velasco, F. Zhang, L. Jing, B. Standley, D. Smirnov, M. Bockrath, A. H. MacDonald, and C. N. Lau, *Proc. Natl. Acad. Sci.* **109**, 10802 (2012).

²⁴B. E. Feldman, J. Martin, and A. Yacoby, *Nat. Phys.* **5**, 889 (2009).

²⁵Z. Liu, K. Suenaga, P. J. F. Harris, and S. Iijima, *Phys. Rev. Lett.* **102**, 015501 (2009).

²⁶J. M. B. Lopes dos Santos, N. M. R. Peres, and A. H. Castro Neto, *Phys. Rev. Lett.* **99**, 256802 (2007).

²⁷E. Suárez Morell, P. Vargas, L. Chico, and L. Brey, *Phys. Rev. B* **84**, 195421 (2011).

- ²⁸H. Min, R. Bistritzer, J.-J. Su, and A. H. MacDonald, *Phys. Rev. B* **78**, 121401 (2008).
- ²⁹C.-H. Zhang and Y. N. Joglekar, *Phys. Rev. B* **77**, 233405 (2008).
- ³⁰M. Y. Kharitonov and K. B. Efetov, *Phys. Rev. B* **78**, 241401 (2008).
- ³¹Y. E. Lozovik, S. L. Ogarkov, and A. A. Sokolik, *Philos. Trans. R. Soc., A* **368**, 5417 (2010).
- ³²A. L. Rakhmanov, A. V. Rozhkov, A. O. Sboychakov, and F. Nori, *Phys. Rev. Lett.* **109**, 206801 (2012).
- ³³P. M. Chaikin and T. C. Lubensky, *Principles of Condensed Matter Physics* (Cambridge University Press, Cambridge, UK, 1995).
- ³⁴I. Sodemann, D. A. Pesin, and A. H. MacDonald, *Phys. Rev. B* **85**, 195136 (2012).
- ³⁵Y. E. Lozovik, S. L. Ogarkov, and A. A. Sokolik, *Phys. Rev. B* **86**, 045429 (2012).
- ³⁶M. Katsnelson, *Graphene: Carbon in Two Dimensions* (Cambridge University Press, New York, 2012).
- ³⁷L. V. Keldysh and Y. V. Kopoev, *Sov. Phys. Solid State* **6**, 2219 (1965).
- ³⁸Y. E. Lozovik and V. I. Yudson, *JETP Lett.* **22**, 274 (1975).
- ³⁹M. Y. Kharitonov and K. B. Efetov, *Semicond. Sci. Technol.* **25**, 034004 (2010).
- ⁴⁰D. S. L. Abergel, R. Sensarma, and S. Das Sarma, *Phys. Rev. B* **86**, 161412(R) (2012).
- ⁴¹See Appendix.
- ⁴²A. MacDonald, J. Jung, and F. Zhang, *Phys. Scr. T* **146**, 014012 (2012).
- ⁴³This type of behavior yields topologically trivial bands, in contrast to some proposals for AB-stacked bilayer graphene. See, for example, Ref. 9.
- ⁴⁴I. L. Aleiner, D. E. Kharzeev, and A. M. Tsvelik, *Phys. Rev. B* **76**, 195415 (2007).
- ⁴⁵P. Olsson, *Phys. Rev. B* **52**, 4511 (1995).
- ⁴⁶J. José, L. Kadanoff, S. Kirkpatrick, and D. Nelson, *Phys. Rev. B* **17**, 1477 (1978).
- ⁴⁷D. Nelson, *Defects and Geometry in Condensed Matter Physics* (Cambridge University Press, New York, 2002).
- ⁴⁸H. A. Fertig, *Phys. Rev. Lett.* **89**, 035703 (2002).
- ⁴⁹See chapter by H.A. Fertig and Ganpathy Murthy in *40 Years of the Berezinskii-Kosterlitz-Thouless Theory*, edited by J. José (World Scientific, New York, 2013).
- ⁵⁰The authors are grateful to Ganpathy Murthy for pointing out this physics.
- ⁵¹Similar physics may be realized in quantum Hall bilayer systems. See L. Radzihovsky, *Phys. Rev. Lett.* **87**, 236802 (2001).